

# Optical and Mechanical Properties of Thin PTFE Films, Deposited from a Gas Phase

Kostyantyn Grytsenko,\* Yurii Kolomzarov, Peter Lytvyn, Olga Kondratenko, Mykola Sopinsky, Iryna Lebedyeva, Agata Niemczyk, Jolanta Baranovska, Dariusz Moszyński, Claus Villringer, and Sigurd Schrader

Thin polytetrafluoroethylene (PTFE) films are produced by deposition from a gas phase by two methods: electron-enhanced vacuum deposition (EVD) and EVD + low-temperature plasma (LTP). Structure, morphology, and composition of the films are studied by IR spectroscopy, atomic force microscopy, and X-ray photoelectron spectroscopy. They are close to the structure of bulk PTFE. The roughness of the films' surface is changed with gas pressure and LTP power variations. Films are transparent from UV to near-infrared regions. Refractive and extinction indices and their anisotropy are measured by spectral ellipsometry. They are tuned by variations of deposition conditions. Hardness and Young modulus of the films are increased if EVD + low power LTP is used for film deposition. Use of EVD + LTP also increases thermal stability of the films. Contact angle of the films corresponds to the bulk PTFE. The PTFE molecules oriented are preferentially in perpendicular direction to the substrate surface.

diodes, field effect transistors,<sup>[11–13]</sup> solar cells,<sup>[14]</sup> and as a matrix for nanocomposite films.<sup>[15–19]</sup> Among the FP, polytetrafluoroethylene (PTFE) has the best thermal and chemical stability. Bulk PTFE is opaque due to the high rate of crystallinity, but thin FP films are transparent in range from UV to near-infrared (NIR) region.<sup>[1–10]</sup> Casting of PTFE film from solution is not possible. The production of PTFE thin film from a gas phase has advantages: deposition onto any substrate or sublayer and co-deposition to produce composite material without restrictions imposed by solubility. Methods of PTFE film deposition from a gas phase could be divided and classified, taking into account precursor, method of its activation, and processes during secondary polymerization (in gas phase or on the substrate

surface). Activation of a fluorinated precursor in a gas phase can be made by various kinds of classical low-temperature plasma (LTP) at a consequent gas pressure.<sup>[8,20–22]</sup> Plasma methods usually led to the formation of crosslinked material with no regular polymer macrochains with repeated monomeric units. Supply of active perfluorinated fragments to substrate surface also can be made with sputtering of bulk PTFE target,<sup>[4,23]</sup> laser or electron beam ablation,<sup>[24,25]</sup> and thermal decomposition of PTFE in a high vacuum.<sup>[11,16,26–29]</sup> The method of evaporation-activation of

## 1. Introduction

Fluoropolymer (FP) thin films attracted attention for their use in optics a long time ago.<sup>[1,2]</sup> Later fluoropolymer films were used in several domains of optics: microlens,<sup>[3]</sup> surface plasmon resonance sensor,<sup>[4,5]</sup> antireflective coatings on plastic optics<sup>[6]</sup> and on alumina,<sup>[7]</sup> waveguides,<sup>[8]</sup> optical recording of information,<sup>[9,10]</sup> etc. Recently, FP films have been used in organic light emitting


K. Grytsenko, C. Villringer, S. Schrader  
Department of Photonic  
Laser and Plasma Technologies  
Institute of Applied Physics  
Technical University of Applied Sciences Wildau  
Hochschulring 1, D-15745 Wildau, Germany  
E-mail: d.grytsenko@gmail.com; kostyantyn.grytsenko@th-wildau.de

K. Grytsenko, Y. Kolomzarov, P. Lytvyn, O. Kondratenko, M. Sopinsky  
Department of Optoelectronics  
Institute of Semiconductor Physics  
pr. Nauky 41, Kyiv 03650, Ukraine

I. Lebedyeva  
Faculty of Mechanics and Mathematics  
Taras Shevchenko University of Kyiv  
64/13 Volodymyrs'ka Str., Kyiv 01601, Ukraine

A. Niemczyk, J. Baranovska  
Department of Materials Technology  
Faculty of Mechanical Engineering and Mechatronics  
West Pomeranian University of Technology in Szczecin  
Szczecin 70-310, Poland

D. Moszyński  
Department of Chemical and Environment Engineering  
Faculty of Chemical Technology and Engineering  
West Pomeranian University of Technology in Szczecin  
Szczecin 71-065, Poland

 The ORCID identification number(s) for the author(s) of this article can be found under <https://doi.org/10.1002/mame.202200617>

© 2023 The Authors. Macromolecular Materials and Engineering published by Wiley-VCH GmbH. This is an open access article under the terms of the Creative Commons Attribution License, which permits use, distribution and reproduction in any medium, provided the original work is properly cited.

DOI: 10.1002/mame.202200617

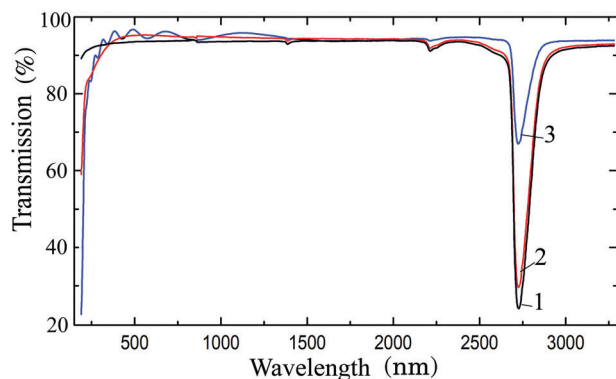


**Figure 1.** Optical transmission spectra of the PTFE films. 1) Quartz substrate, 2) 96 nm thick, 3) –625 nm thick.

PTFE in a high vacuum (electron-enhanced vacuum deposition (EVD)) was used for production of active fluorinated volatile fragments by thermal decomposition of bulk PTFE and electron impact with emitted fragments in a gas phase.<sup>[11,16]</sup> Produced films had a structure close to bulk PTFE and consisted of mainly linear macromolecules, however, they did not have enough thermal stability. They changed their structure and refractive index during annealing at 220 °C.<sup>[28]</sup> Controlled modification of the PTFE film structure and properties was made with additional not self-sustained radio frequency (RF) LTP at a comparatively low pressure and power in gas of the fluorofragments during EVD.<sup>[11,28]</sup> The smoothness and optical transparency of the PTFE films, deposited by EVD seems high enough for their applications in optoelectronics.<sup>[11]</sup>

The aim of this work is the control of the optical and mechanical properties of the PTFE films by variations in deposition conditions.

## 2. Results and Discussion

Optical transmission spectra of the PTFE films deposited by EVD are shown in **Figure 1**. They are close to optical spectrum of polyhexafluoropropylene (Teflon-FEP) thin industrial film.<sup>[30]</sup> Optical spectra are also close to spectra of thin films produced by thermal evaporation of PTFE in a vacuum,<sup>[31]</sup> by RF sputtering<sup>[32]</sup> and produced from a gas phase.<sup>[33]</sup> Produced films are more transparent than produced by pulsed laser deposition,<sup>[34]</sup> by RF plasma polymerization<sup>[8]</sup> or magnetron sputtering.<sup>[35]</sup> It seems that films produced by plasma at a comparatively high RF power had a smaller transmission. Films deposited by EVD were completely transparent from the UV via the visible to the NIR region. Absorption edge was near 190 nm. PTFE films exhibited an antireflective effect on the absorption of the quartz in the visible region. Strong decrease of the band located nearby 2700 nm which is attributed to (-OH) groups can be related with a decrease in their concentration. It is known that pressure of the evaporated fragments influenced the refractive index of PTFE films.<sup>[28]</sup> Refractive index of the PTFE films deposited by EVD versus pressure of evaporated fragments are shown in **Table 1**. The elevation of the pressure from  $10^{-4}$  to  $10^{-3}$  mbar led to a decrease in the refractive index from 1.37 to 1.15. The extinction coefficient was increased more

**Table 1.** Refractive index of PTFE films (632 nm) versus pressure of the gas.

No.	Pressure [mbar]	Thickness [nm]	Refractive index	Extinction coefficient
1	$3 \times 10^{-5}$	760	1.38	0.0002
2	$2 \times 10^{-4}$	230	1.375	0.0017
3	$8 \times 10^{-4}$	120	1.335	0.0024
4	$8 \times 10^{-4}$	300	1.34	0.0016
5	$2 \times 10^{-3}$	210	1.25	0.0025
6	$2 \times 10^{-3}$	1200	1.25	0.0021
7	$4 \times 10^{-3}$	200	1.15	0.0034
8	$4 \times 10^{-3}$	320	1.16	0.0038

than ten times. This was the result of formation of porous and disordered PTFE material.

Annealing of the PTFE films deposited by EVD led to the increase of their refractive index, while films deposited by EVD + RF LTP kept refractive index unchanged.<sup>[16,28]</sup> The refractive index increase showed densification of the film during heating. The thicker PTFE film had higher refractive index,<sup>[11]</sup> but in ref. [36] it was shown that refractive index of the PTFE film had a minimum at a certain film thickness.

During next research stage, optimal conditions for production of transparent PTFE films with stable refractive index were searched. The multiparametric system of deposition conditions included the pressure of emitted fragments, power of RF LTP, a fixed or rotated substrate. Deposition conditions and thickness of the PTFE films, produced by EVD and EVD+ RF LTP are presented in **Table 2**.

### 2.1. Atomic Force Microscopy (AFM) Studies of the Films Surfaces

AFM images of PTFE films deposited with different pressures are presented in **Figure 2**. Microparticles with a shape close to the sphere appeared in the films deposited at comparatively high pressure of emitted fragments both during pure LTP or EVD only. At a high pressure, microdrops were formed in the gas phase due to impacts and reaction of active fragments. Produced drops were condensed on the substrate surface. Films deposited by EVD showed a decrease in surface roughness with a pressure decrease even at a low pressure when no microdrops were formed. The surface of the EVD PTFE thin film represents bumps with a length of about 70 nm with a roughness of about 8 nm. The thicker the PTFE film, the bigger the surface roughness is. The formation of the observed surfaces was the result of the Volmer–Weber growth mechanism. **Figure 3** shows the influence of pressure and RF power of LTP during EVD to morphology and relief of PTFE films at a comparatively low pressure.

RF LTP during EVD at low pressure slightly decreased the surface roughness of the PTFE film as compared with that deposited by EVD only. The increase of pressure and decrease of plasma power led to an increase of PTFE surface roughness. LTP at a high pressure increased surface relief. Low-power LTP acted on the film morphology in two counter directions: it produced smaller active fragments which led to an increase of the film growth rate

**Table 2.** Deposition conditions and characterization of PTFE films.

Sample no.	Pressure [mbar]	RF power [W], accepted		Thickness AFM [nm]	Thickness ellipsom. [nm], ISP	Thickness ellipsom. [nm], TH Wildau
14	$2 \times 10^{-4}$	0	fixed	210	215	-
15	$2 \times 10^{-4}$	0	rotated	190	207	182.5
16	$2 \times 10^{-4}$	0	fixed	1010	1113	1061.4
17	$3 \times 10^{-4}$	50	rotated	145	155	156.4
18		Annealed at 80 °C No 17		157	168	160.4
19	$2 \times 10^{-4}$	50	fixed	253	-	-
20		Annealed at 80 °C No 19		237	-	-
28	$9 \times 10^{-4}$	50	fixed	470	509	443.5
29		Annealed at 80 °C No 28		461	510	463.6

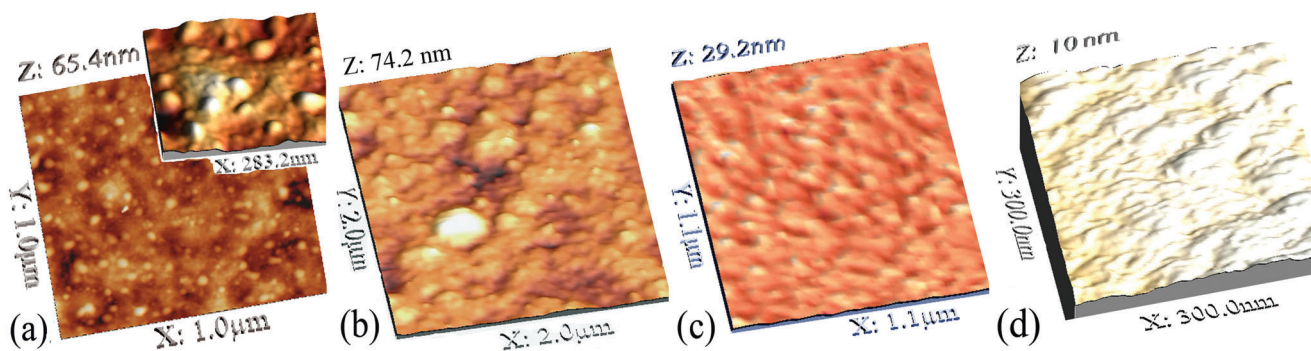


**Figure 2.** Morphology of 50 nm thick PTFE films, deposited at pressure: a) 50 Hz plasma,  $5 \times 10^{-2}$  mbar; EVD; b)  $9 \times 10^{-3}$  mbar, c)  $1 \times 10^{-3}$  mbar, d)  $4 \times 10^{-4}$  mbar.

and crosslinks, thus keeping the material in a nonequilibrium state, preserving it from the formation of supermolecular structure; at a high pressure, smaller active fragments promoted the growth of microparticles in a gas phase. Therefore, a combination of pressure and plasma power has a nonlinear influence on the smoothness of PTFE films. In films 17 and 18, the periodic-oriented superstructure was detected (Supporting Information). Annealing led to an increase of roughness of film 17 but not of film 28. The optimal properties of PTFE film could be defined as such at which the film is most transparent, its refractive index and extinction coefficient are small and stable.

## 2.2. Optical Properties of the Films

Optical transmission spectra of PTFE films deposited with LTP are shown in **Figure 4**. Spectra of the films deposited at high pressure with 50 Hz plasma had absorption in visible and NIR regions, sharply increased in the blue region. The films had yellow color. Transmission of all PTFE films deposited by EVD + RF LTP was between 90% and 100% in the visible region. The PTFE films exhibited an antireflection effect for a quartz substrate. The PTFE film deposited at lowest pressure with 50 W RF LTP showed a transmission increase after annealing. PTFE films deposited at intermediate pressure by EVD + LTP showed no changes in transmission after annealing. Perfluoropolymer films deposited by magnetron sputtering (300 W 40 kHz) on glass at room tem-

perature showed a similar transmission increase.<sup>[37]</sup> The heating of the films but to a higher temperature allowed the transmission to return to the value of bare glass. The perfluoropolymer coating on multilayered inorganic film also led to its transmission increase.<sup>[38]</sup> Therefore, at optimal conditions, the EVD, EVD + LTP, and pure plasma methods allow to produce transparent perfluoropolymer films in the visible region.

The changes in refractive indices  $n(\lambda)$  of the as-deposited films and after annealing were estimated in the range from 250 to 2100 nm using the isotropic model. The refractive indices are shown in **Figure 5a–c**. The thickness of PTFE films was found for each ellipsometry fit (Table 2).  $n(\lambda)$  dependencies of the films show normal dispersion. The refractive index increases as the wavelength of light decreases. According to the isotropic model, the shape and slope of the curves and values of refractive index for all films were close. Starting from about 1.32 in NIR region, the refractive index of films increases up to 1.36–1.37 in the UV region. The increase in the refractive index of film 28 after annealing was very small. The thickness of film 28 was not changed as measured by AFM and ellipsometry in ISP, Kyiv. The refractive index of the films is higher than for films produced by catalytic chemical vapor deposition<sup>[39]</sup> and by electron beam ablation.<sup>[40]</sup> The higher refractive index for deposited PTFE films is originated from a more dense film structure. This is clearly seen from comparison of the figures concerning surface topology in this research and in refs. [39, 40].

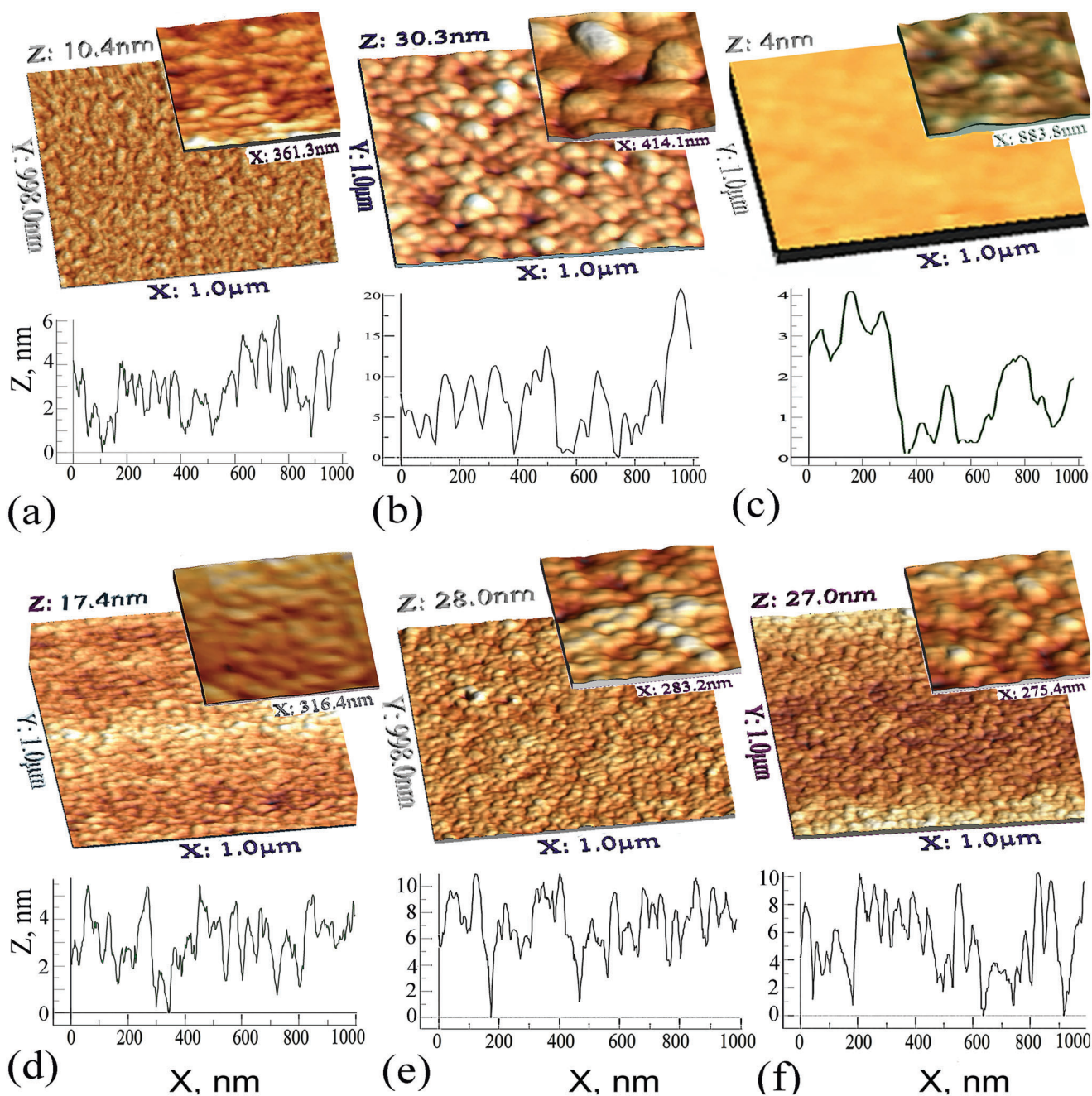


**Figure 3.** Influence of pressure, RF power, and annealing on morphology of PTFE films. a)  $3 \times 10^{-4}$  mbar, 50 W (film 17); b)  $1 \times 10^{-3}$  mbar, 20 W; c)  $2 \times 10^{-4}$  mbar, 20 W, insert with increased Z magnification; d) is annealed a) (film 18); e)  $9 \times 10^{-4}$  mbar, 50 W (film 28); f) is annealed e) (film 29).

The refractive indices and absorption coefficients of the films were calculated as anisotropic in planes parallel and perpendicular to the substrate surface (Figure 5d–i). For refractive indices of films 15 and 16, a very small anisotropy in UV and small anisotropy in vis-NIR regions were found out. The refractive index in perpendicular direction to surface plane was a little bigger than in parallel. The refractive index values were about 0.005 bigger than values obtained by the isotropic model. For films 28 and 29, the refractive index was started from almost 1.4 in UV and still bigger than that obtained from the isotropic model in visible

region. The refractive index of the film 28 was slightly decreased after annealing, while the change of  $n$  for 17 was very small. The anisotropy of the films deposited by EVD is two to three times bigger than the anisotropy of the fluoropolymer films produced from a liquid phase for waveguide.<sup>[41]</sup> The anisotropy of the films deposited by EVD + RF LTP is three times bigger.

The extinction coefficient for the films was small in the range from 0.006 in UV to almost 0 in NIR region. For film 16, it was as small as extinction coefficient for industrial Teflon-FEP film.<sup>[30]</sup> For all films, the extinction coefficient was bigger in a

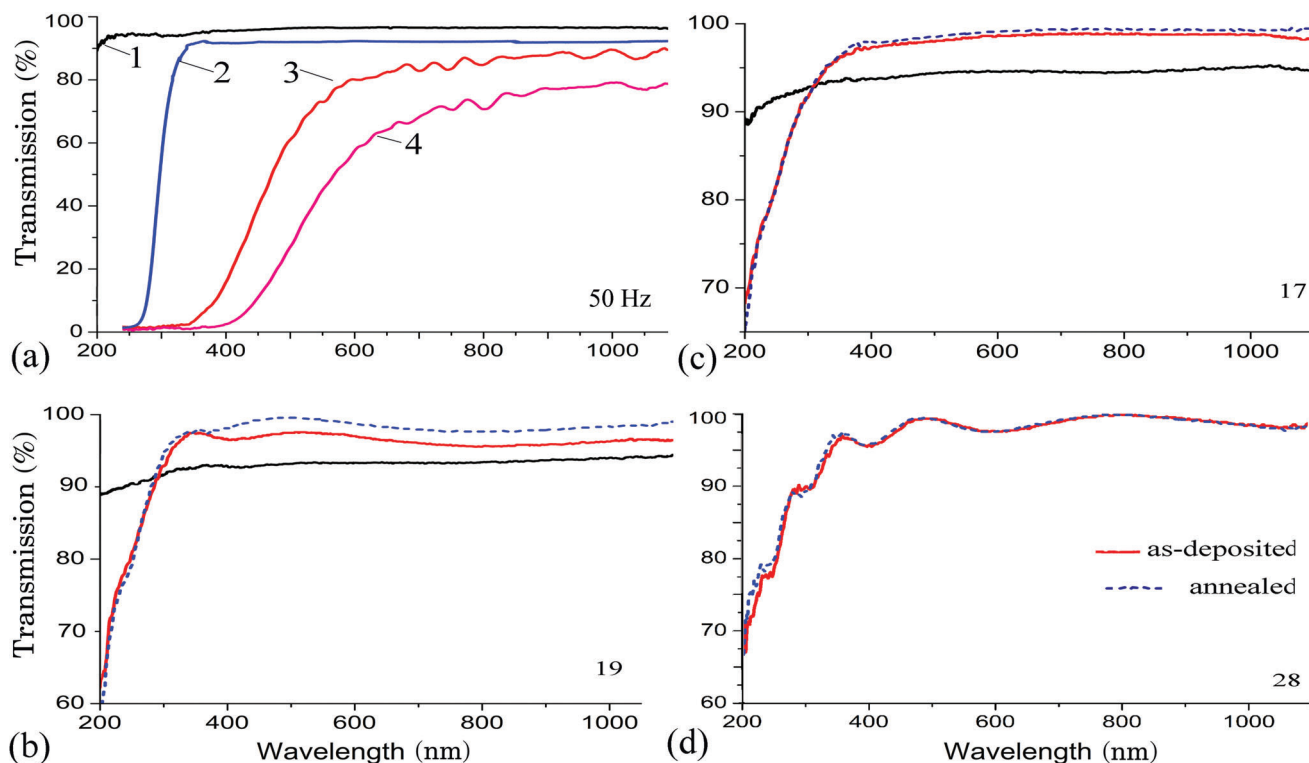


**Figure 4.** Optical transmission spectra of PTFE films, deposited with LTP. a) 50 Hz plasma, 1: quartz, 2: glass, 3: thinner film, 4: thicker film; b)  $2 \times 10^{-4}$  mbar, 50 W, films 19 and 20; c)  $3 \times 10^{-4}$  mbar, 50 W, films 17 and 18; d)  $9 \times 10^{-4}$  mbar, 50 W, films 28 and 29. Solid lines: black: quartz substrate, red: as-deposited, dotted blue: annealed films.

perpendicular direction and slightly increased after annealing. The extinction coefficient for films deposited by EVD + RF LTP revealed a sharp increase in the UV region as compared with films produced by EVD only. The extinction coefficient of all films was significantly smaller than the extinction of industrial “thick” PTFE film. Small differences in the data measured in ISP, Kyiv and in TH Wildau can be explained by the different models used for the calculations of  $n$  and  $k$ . The density of the all PTFE films in direction perpendicular to the film surface is bigger than in parallel directions.

The refractive index dispersion data below the fundamental interband absorption edge of many covalent and ionic compounds are well described by the Wemple and DiDomenico single effective oscillator model (W-D) with two parameters  $E_0$  and  $E_d$ <sup>[42]</sup>

$$n^2(h\nu) = 1 + E_0 \cdot E_d / [E_0^2 - (h\nu)^2] \quad (1)$$

The parameter  $E_0$  is single-oscillator energy (the average excitation energy for electronic transitions) that characterizes an average energy gap. The parameter  $E_d$  is the single oscillator strength or dispersion energy which is a measure of the strength of interband optical transitions. To establish how well the dispersion of our films is simulated by the W-D model, experimental dispersive  $n(h\nu)$  dependences as  $1/(n^2 - 1)$  versus  $(h\nu)^2$  were built. Figure 5j demonstrates such dependences for films 15 and 16. For the film 16, dispersive  $n(h\nu)$  dependence is described by the W-D model in all spectral range (1.34–4.13 eV) for the light with the electrical vector oscillations direction both perpendicular and parallel to

**Table 3.** Parameters of the W-D model for the PTFE films.

Sample no.	$E_0(z)$ [eV]	$E_0(xy)$ [eV]	$E_d(z)$ [eV]	$E_d(xy)$ [eV]
16	13.76	13.76	11.17	11.08
15	10.5	11.7	8.4	9.3
28	13.22	13.06	11.25	10.77
29	13.23	13.16	10.74	10.37

the film surface. For this film, the values of parameters  $E_0$  and  $E_d$  have been obtained from linear fitting of  $1/(n^2 - 1)$  versus  $(h\nu)^2$  dependences in full spectral range. Their values are given in **Table 3**. The values for both  $z$  and  $xy$  directions are almost the same. In contrast to this, in film 15 the range of fulfillment of dependence (1) is narrowed for both directions of the light wave electric vector oscillations. It indicates that in this film the tail of absorption spectrum is more extended (and greater in magnitude). The growth of this long-wavelength absorption was due to increased density of states in the band gap as a result of the increase in the number of structural defects in film 15. For determination of  $E_0$  and  $E_d$  in film 15, a linear fit of low energy part of the  $1/(n^2 - 1)$  versus  $(h\nu)^2$  dependences was used. The values of  $E_0$  and  $E_d$  are given in Table 3. For the film 15, the values of both  $E_0$  and  $E_d$  are different for  $z$  and  $xy$  directions. Wemple and DiDomenico<sup>[42]</sup> and Tanaka<sup>[43]</sup> suggested that W-D effective oscillator energy  $E_0$  relates to the optical band gap  $E_g$ . Tichá and Tichý<sup>[44]</sup> examined the correlation between  $E_g$  and  $E_0$  for 42 compounds where  $E_g$

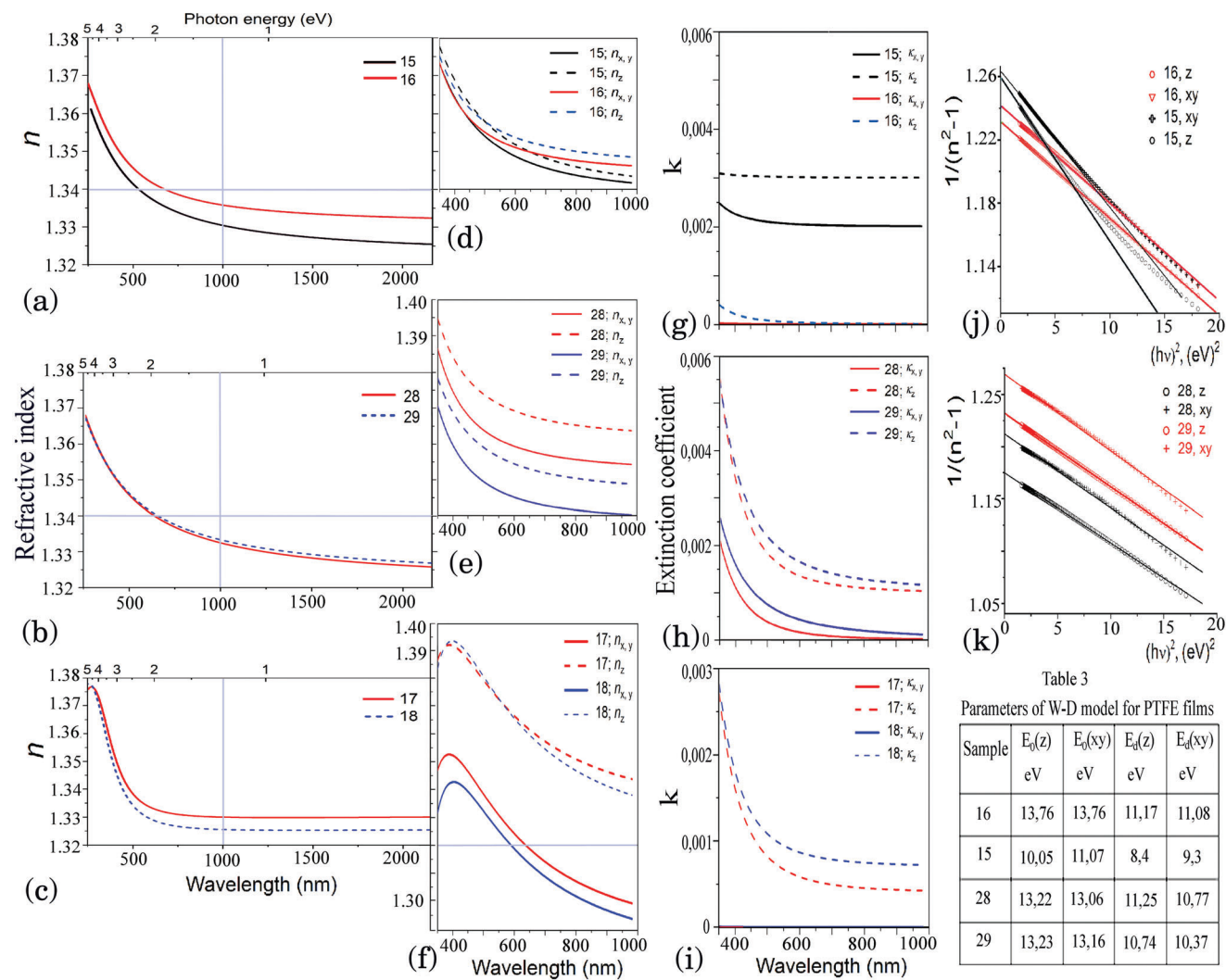


**Figure 5.** Refractive indices of PTFE films. a–c) In range from 250 to 2100 nm. Solid line as-deposited films, dash line annealed films; d–f) refractive indices and g–i) extinction coefficients of films in perpendicular and parallel directions to substrate in range from 300 to 1000 nm; j,k) dispersion of the  $n_z$  and  $n_{xy}$  based on the Wemple–DiDomenico model.

values lie within a broad interval from 0.18 (InSb) to 13.6 eV (LiF). They found that the correlation  $E_0(E_g)$  can be expressed:  $E_0 = 1.25 \cdot (1.2 + E_g)$ . Thus, an approximate value of the optical band gap  $E_g$  can be obtained from the W-D model. Using the relation between  $E_0$  and  $E_g$ , such estimates for  $E_g$  are obtained: for the film 16,  $E_g(z) = E_g(xy) \approx 9.9$  eV, for the film 15,  $E_g(z) \approx 7.2$  eV,  $E_g(xy) \approx 8.2$  eV. The values of  $E_g$  for the film 15 are smaller than for the film 16. Both absorption and scattering can contribute to nonzero extinction coefficient. The scattering dominated in the film 16, but the absorption on defects was dominant in the film 15 (Supporting Information).

For films 28 and 29, the  $n_z(h\nu)$  dependence is well described by the W-D formula in all spectral range (Figure 5k). For the  $n_{xy}(h\nu)$  dependence, deviation from this rule in high-energy part of the range was observed. Parameters of this model are given in Table 3. Annealing caused a small change of  $E_0(z)$  and  $E_0(xy)$ . In the as-deposited film,  $E_0(z)$  is larger by 0.14 eV,  $E_0(z)$  and  $E_d(z)$  is larger by 0.48 eV per  $E_d(xy)$ . Annealing did not change  $E_0(z)$ , but

increase  $E_0(xy)$  by 0.1 eV. The  $E_d(z)$  and  $E_d(xy)$  values decreased by 4–5% after annealing. Annealing brings the values of  $E_0$  and  $E_d$  for z- and xy-direction closer.  $E_g$  was estimated for the film 28:  $E_g(z) = 9.38$  eV,  $E_g(xy) \approx 9.25$  eV, for 29  $E_g(z) = 9.38$  eV,  $E_g(xy) \approx 9.33$  eV. For the films 28 and 29, there is a difference in the dominant contributions to the extinction coefficient for the xy- and z-directions (see Supporting Information). If for the z-direction the absorption contribution dominates, for the xy-direction the small dominance of scattering in the as-deposited film and its almost complete dominance in the annealed film are observed.

### 2.3. IR Spectroscopy (IRS) and X-Ray Photoelectron Spectroscopy (XPS) Studies of Film Structure and Composition

First IRS studies of the structure of PTFE date back to the 1950s.<sup>[45,46]</sup> IRS of bulk PTFE were described in several papers.<sup>[47–51]</sup> The seemingly simple to model and analyze

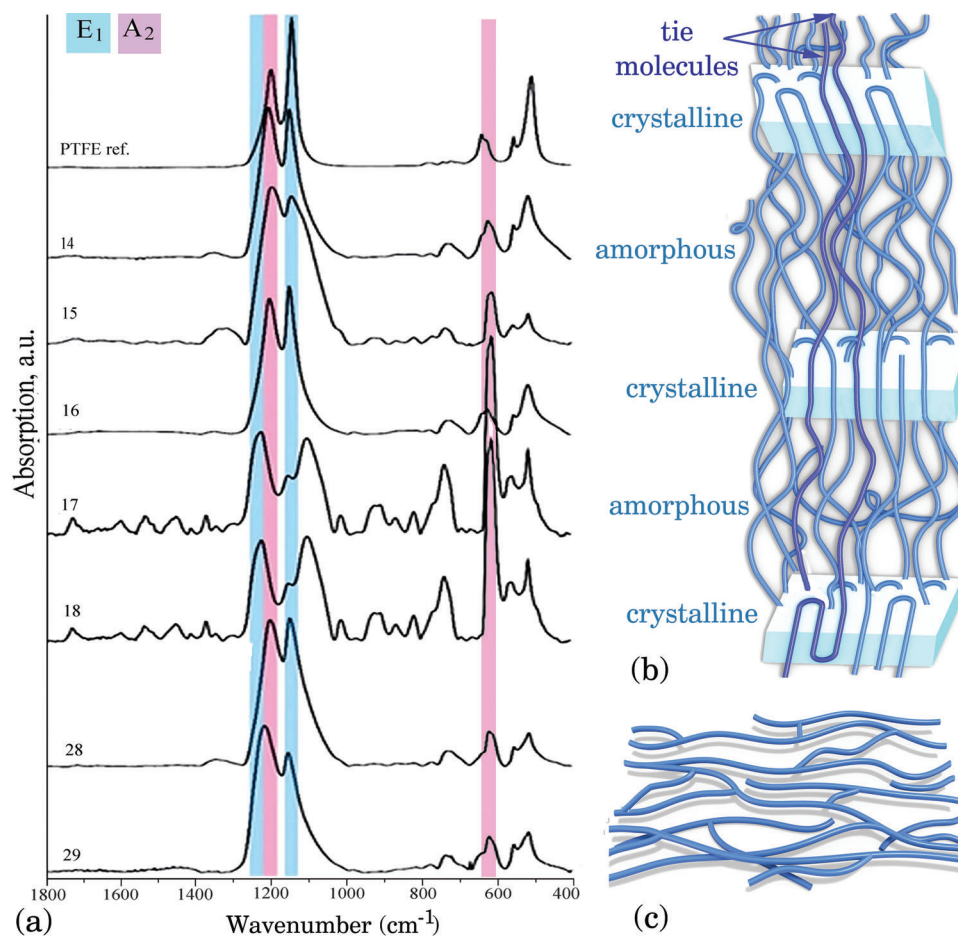


**Figure 6.** a) IRS of the PTFE films deposited by EVD and EVD + RF LTP. Simplified structure of the films: b) ensemble of amorphous and crystalline domains with polymer chains oriented in direction perpendicular to substrate surface (15, 16, 28, 29), c) irregular structure of crosslinked plasma perfluoromaterial with chains oriented in direction parallel to substrate surface (in 17, 18).

molecular structure of this polymer, consisting only of  $(-CF_2-)$  repeating units, still raises plenty of debate and uncertainty, especially in the fingerprint region and wavelengths around  $800\text{--}400\text{ cm}^{-1}$ . Most inconsistency in the authors' experimental observations and simulations is in the origin of changes in the absorption intensity of the bands at  $600\text{--}650\text{ cm}^{-1}$ , i.e., if they occur due to a change in the crystallinity degree or due to defects in conformation of the PTFE helix.<sup>[50]</sup> The shape and intensity of bands of PTFE IRS are influenced by many factors: concentration of amorphous phase, orientation of the macromolecules,<sup>[51–56]</sup> presence of various chain conformations,<sup>[50,57]</sup> crosslinks, side groups, defects, and strain. **Figure 6** shows IRS and chemical composition (**Table 4**) of the PTFE films deposited at various conditions. **Table 5** presents relative intensity of the IRS bands. More detailed tables concerning IRS of each film are in the Supporting Information. Main bands of IRS of the all deposited films correspond to bands of IRS of PTFE films deposited from a gas phase<sup>[52,56–58]</sup> and bulk PTFE. But IRS of PTFE films deposited by EVD or by EVD + RF LTP showed featured differences. Nevertheless, in terms of thin films, the orientation of PTFE chains can be assessed by the analysis of the particular absorption bands intensity, specifically the bands whose dipole moment of vibrations

**Table 4.** Composition of the film surfaces.

No.	C	F	F/C
Ref.	31.9	68.1	2.13
14	33.2	66.8	2.01
15	29.9	70.1	2.34
16	29.7	70.3	2.37
17	31.0	69.0	2.23
18	31.7	68.3	2.15
28	31.6	68.4	2.16
29	30.5	69.5	2.28

is perpendicular to the axis of molecules, i.e.,  $E_1$  type symmetry and the bands which have a dipole moment of vibration parallel to axis of a molecule, i.e.,  $A_2$  type of symmetry. The most intensive  $E_1$  and  $A_2$  fundamental absorption bands observed for PTFE films, as well as for the reference material, are at  $1146\text{ cm}^{-1}$  (assigned to  $CF_2$  symmetrical stretching vibration,  $E_1$ ), at

**Table 5.** Relative intensity of the IRS bands of the PTFE films.

Wavenumber [cm <sup>-1</sup> ]	Assignment	Relative intensity [%]						
		14	15	16	17	18	28	29
505–515	CF <sub>2</sub> in crystal	10.4	7.4	11.3	6	6	6.7	7.2
600–608		6.1	9.2	7.8	45	47	4.9	5.3
612–619		6.5	3.4	8.2	42	43	5.1	5.4
766–780	Crystal	1.0	0.4	1.4	4.4	4.3	0.8	1.4
814–819	Amorphous	-	1.2	1.2	3.8	4.4	0.5	0.8
862–867	Amorphous	0.8	-	-	2.7	2.8	-	-
906–909	Crosslinks	-	1.1	-	4.2	4.4	-	-
929–933		-	1.1	-	4.3	4.1	-	-
982	-CF <sub>3</sub>	-	-	0.7	-	-	-	-
1019–1036	branches	0.9	2.0	-	3.2	3.6	0.9	1.5
1062–1084	branch or helix defect	-	1.4	-	5.1	5.1	2.4	-
1098–1104		7.0	-	5.3	15.9	18.1	10.2	6.9
1019–1125		10.4	2.0	8.5			8.3	6.8
1148–1152	CF <sub>2</sub> E1	23.1	15.6	25.8	6.1	6.7	22.7	15.6
1171–1175		13.6	11.3	11.9	4.0	4.3	11.3	10.8
1201–1210	CF <sub>2</sub> A2	27.8	22.8	27.2	7.4	7.6	26.2	21.1
1234–1237	C–C E1	11.9	8.1	8.3	14.9	14.1	8.8	15.8
1294	CF	-	-	-	1.3	0.6	-	-
1311–1324		-	2.4	-	1.3	0.8	0.8	-
1345–1350	CF <sub>3</sub>	1.1	1.7	-	1.4	1.3	1.4	-
1373	CF <sub>3</sub>	-	-	-	3.1	3.2	-	-
1411–1422		-	-	-	1.0	1.4	-	0.7
1449–1439					2.6	2.5		0.6
1471–1473	C=C				1.7	1.3		0.9
1532	(crosslinked				2.9	2.5		
1600	part of chain or in aromatic)				2.1	1.5		
1659	-CF=C<				1.0	-		
1711	-CF=CF-		0.8		1.2	1.0		
1730	-CF=CF-				2.6	2.2		

1200 cm<sup>-1</sup> (assigned to CF<sub>2</sub> asymmetric stretching vibration, A<sub>2</sub>), and at 1235 cm<sup>-1</sup> (assigned to C–C chain backbone stretching vibration, E<sub>1</sub>). For all examined films, the E<sub>1</sub>:A<sub>2</sub> ratio has been changed and the A<sub>2</sub> band becomes the dominant band. It indicates that in films a higher amount of PTFE chains is aligned perpendicularly than parallelly to the substrate surface. Such PTFE film growth is well recognized for coatings produced from active gas phase.<sup>[50]</sup> The macromolecules in the first “layers” of the PTFE film (thickness below 20 nm) are poorly ordered and aligned rather parallel to substrate surface. After reaching a certain thickness of the film, chains start to grow in a perpendicular orientation with a certain tilt also dependent on film thickness.<sup>[52]</sup>

IRS of all three films (14, 15, 16) deposited by EVD have all characteristic PTFE absorption bands indicating that the structure of the polymer has been preserved. Nevertheless, some new low-intensity bands are also present in the spectra and, what is more, the intensity ratio of CF<sub>2</sub> bands is different in comparison to reference material. The proportion of the E<sub>1</sub> band at 1146 cm<sup>-1</sup> (1149 for 14, 1147 for 15, and 1148 cm<sup>-1</sup> for 16) to A<sub>2</sub> band at 1200 cm<sup>-1</sup> (1205, 1201, 1203 cm<sup>-1</sup>, respectively) is

lower and almost equals 1 (for reference PTFE it was 1.5). It indicates that the films are mostly consisted of the perpendicularly arranged macromolecules. Bands present in the region 1100–900 cm<sup>-1</sup> evidence some branching or crosslinking of the PTFE chains, which are especially noticeable for film 16. This coating is also characterized by a higher (comparing to reference material and films 14, 15) amount of the CF<sub>3</sub> groups, which occurrence is likely a consequence of branched chains. Considering the fact that the main difference between coating 14 and 15 is the rotation during the deposition, it can be concluded that this process parameter affects the level of branching/crosslinking of PTFE coating. Film 16 has the most similar structure to reference material, having only a small level of the chain branches. It is probable that comparatively branched structure was created only at the beginning of the EVD deposition process (like ref. [52]) and the rest of the film was built without chain distortion. Chain growth through the addition of successive CF<sub>2</sub> groups is the most energetically beneficial. Thinner films, such as 14 and 15, might have a higher relative intensity percentage of the bands origin from the branching because its amount in relation



to the total mass of the film is greater. The films 17 and 18 deposited by EVD + RF LTP have all the characteristic bands of PTFE with weaker comparative intensity, but also a large number of additional bands that indicate the main chain is branched, the chains are crosslinked at a certain degree and unsaturated ( $-C=C-$ ) bonds are present. The significant increase in the amorphous phase is reflected by new bands in the  $900-800\text{ cm}^{-1}$  region and in intensity of band at  $767\text{ cm}^{-1}$ , which is almost four times greater than for reference PTFE. Due to high quantity of the additional bands, the estimation of the spatial arrangement of the macromolecules by the analysis of the  $E_1:A_2$  ratio can be flawed by a large error. It can be suggested from intensive band located at  $607-615\text{ cm}^{-1}$  that in the films 17 and 18 concentration of the macromolecules oriented parallel to substrate surface is bigger than that in other films. The like IRS was recorded in ref. [56] for PTFE film grown by EVD + RF LTP. But with strong decrease of the  $E_1\text{ CF}_2$  bands and moderate decrease of  $A_1\text{ CF}_2$  band, the band nearby  $610\text{ cm}^{-1}$  was not increased. Therefore, in film deposited in ref. [58], the decrease of  $\text{CF}_2$  groups was caused by crosslinking, but not by molecules oriented parallel to the surface.

The annealing of the film (17 vs 18) decreased relative intensity of bands originating from unsaturated carbons ( $1400-1500$  and  $1600-1750\text{ cm}^{-1}$ ). In the as-deposited film 17, polymerization process was not finished. In the film still available free dangling bonds and low molecular oligomers. The annealing allowed to polymerize material to a higher degree, but not to completely finish it. The extended composition of the functional groups in the film was due to deposition by EVD + RF LTP. The additional LTP with parameters used for deposition of film 17 produced strongly destructed fragments with two or three free bonds. Their participation in film growth led to the formation of branched and crosslinked polymer chains, sometimes with an open bond at the end or in the middle of chain. Other changes in IRS were small. Therefore, the structure of film 17 was preserved during annealing.

IRS of films 28 and 29 is characterized by all typical PTFE bands. The bands, which indicate chain branching and crosslinking, are on a low level. The deposition parameters of the EVD + LTP during production of film 28 were favorable for the creation of small fragments with a structure close to diradical ( $-C_2F_4-$ ) without fragments destructed more strongly. The changed  $E_1/A_2$  ratio after annealing indicating higher level of chains arranged perpendicular to the substrate surface. This confirms low crosslinking of the film.

The elemental composition of the film surfaces calculated based on the results of XPS analysis is presented in Table 4. The surface consisted only of fluorine and carbon, and the F/C ratio calculated as the quotient of the respective surface compositions (in atomic percent) for the films and reference material is ranging from 2.01 to 2.37. Very close F/C ratio and the shape of the C 1s and F 1s spectra of the coatings and the reference material confirmed that the chemical structure of PTFE has been preserved. In terms of the influence of the annealing on the structure of the films, the two groups can be recognized. For films 17 and 18, the F/C ratio has been decreased after annealing and for films 28 and 29, the F/C ratio has been increased. A change in the spatial conformation of the chain can change the elemental composition of the first layers of the film surface.

## 2.4. Films Mechanical Properties

Figure 7 shows mechanical properties of the PTFE films. The hardness and Young's modulus of the films deposited by EVD+RF LTP depend on fluorofragments pressure and were higher than that of the films deposited by EVD only. The hardness of rotated film 17 was bigger than that of fixed 19. This effect can be due to the small plasma species that can participate in the film growth even in a shielded zone, leading to more crosslinked structure of the film. The films deposited by EVD+RF LTP revealed a smaller penetration depth and a larger segment of elastic deformation in the loading curve. The comparatively low hardness of film 28 can be due to the low crosslinking of the film, which is related directly.<sup>[59]</sup> The mechanical properties of the PTFE films deposited with EVD+ LTP are comparable with the properties of the films produced by classic plasma methods summarized in ref. [60]. After annealing, the hardness of film 17 deposited at a low pressure became smaller. This can be due to the small swelling of the film. The quantity of crosslinks was not good enough to overcome the influence of many defects.

## 2.5. Advancing Contact Angle

Advancing contact angle of the films is shown in Figure 8. Reference PTFE has  $\theta_a$  equal  $115^\circ$  and the films have  $\theta_a$  in range  $106^\circ-128^\circ$ . Dynamic contact angle can be influenced either by the chemistry of the surface (by the changed elemental composition) and by the film topography.

Because the composition changes are on a low level and as no correlation of the angle value and XPS results have been found, it can be assumed that they are caused by the different roughness of the film surfaces.<sup>[61,62]</sup> The annealing of all films led to increased  $\theta_a$  value. Small increase of the  $\theta_a$  value in the films 17 and 18 can be caused by roughness increase, but in the films 28 and 29 the roughness was not changed, only concentration of F on the surface was increased a little.

## 2.6. Final Discussion

The morphology, structure, the orientation of polymer chains, optical and mechanical properties of thin PTFE films were varied via deposition methods and their parameters. The deposition parameters influenced properties of the PTFE film in complex interrelated ways.<sup>[63]</sup> The properties of the PTFE film depend on the pressure of perfluorinated fragments in chamber, deposition rate, rotation of substrate, and power of additional RF LTP. In general, the growth process starts from fragment adsorption, chemisorption, and surface diffusion to find a partner to form the nucleus. Here, the ratio between thermodynamic (system: gas phase – substrate – solid phase) and kinetics (rate of fragment supply) plays a role. The substrate temperature had to be sufficient for fragment diffusion, but not too high for their re-adsorption during the time necessary for fragments to collide with each other and react. The smaller the rate of fragments supply is, the more in equilibrium are the processes, and a higher molecular mass of the film is expected. At the beginning of this stage (before formation of the monolayer), the orientation of

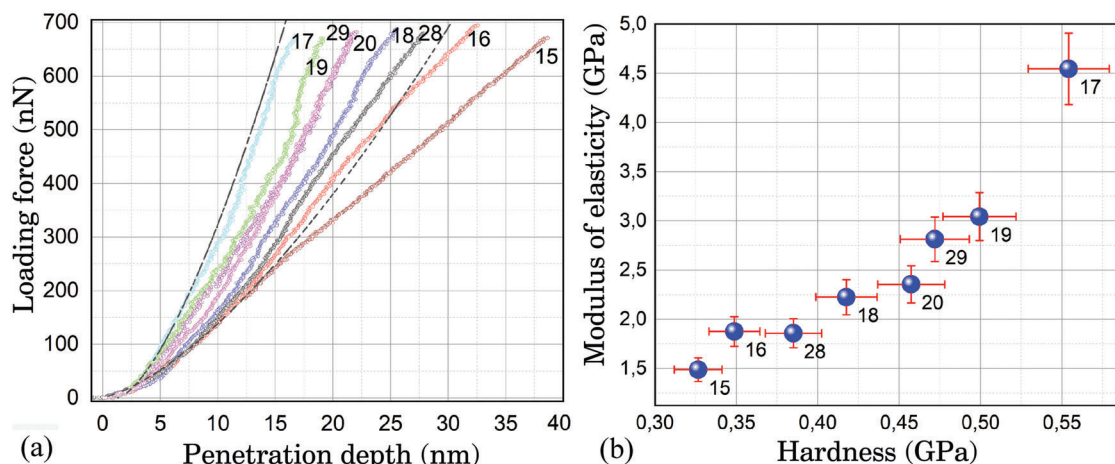


**Figure 7.** Nanomechanical testing of PTFE films. a) Load-penetration curves for the PTFE films. Dashed black lines indicate the Hertz model fitting for films 17 and 15. b) Elasticity modulus versus hardness.

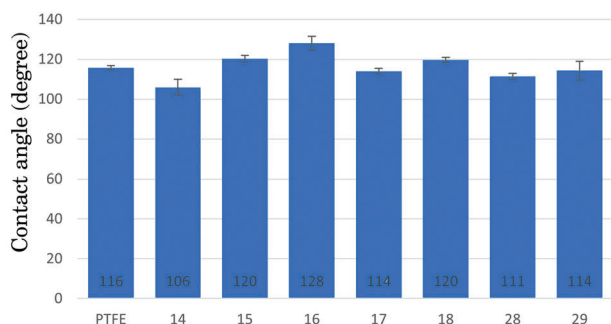


**Figure 8.** Advancing contact angle of the water drop on the PTFE films.

small fragments is expected to be in the plane of the substrate surface. At a certain film thickness, the oligomeric chains can stand up in a direction perpendicular to the surface, if the intermolecular interaction is stronger than the molecule–substrate interaction. The possible differences in the film structure caused by properties of the Si or quartz substrates should be taken into account during the comparison of IRS and optical data. Crosslinking suppresses any material transformation. Perhaps film 17 has enough quantity of short pieces of molecular chains, frozen parallel to the substrate surface by crosslinking (Figure 6b). Further film thickness growth leads to the formation of crystal and amorphous nanodomains. Crosslinks quantity again influences the material organization. The next step in the formation of supermolecular structure certainly needs a more thick film (estimated as 100 nm for polyethylene, etc.<sup>[16]</sup>). The ensemble of the crystal and amorphous domains can form self-organized structures. The bulk PTFE was considered as consisting of three phases: mobile amorphous, rigid amorphous, and crystalline.<sup>[64]</sup> The strongly crosslinked material can be considered as the fourth phase. The amorphous phases can have preferential aligning of polymer chains as it was proposed for polyethylene.<sup>[65]</sup> Films 15, 16, 28, and 29 contain chains oriented preferentially perpendicular to the substrate surface. Perhaps the crystals with oriented chains formed ensemble with preferential orientation of rigid amorphous phase where the concentration should be bigger as

compared with its concentration in bulk PTFE (Figure 6a). An increase in film 28 hardness as compared with films 15 and 16 can be due to longer chains and small quantity of crosslinks. Orientation of chains in rigid amorphous phase in direction perpendicular to the surface led to an increase of hardness more than tenfold.<sup>[66]</sup> The hardening of film 28 after annealing was due to finishing of polymerization of free dangling bonds. Decrease in hardness of film 17 after annealing can be due to bonds breaking and structure damage perhaps due to high inner stress. The hardness of films was increased by use of the EVD + low power RF LTP method due to partial crosslinking. The crosslinks quantity in films 28 and 29 is far smaller than for films produced by classic plasma. Thin PTFE films have hardness about five times bigger than that of bulk PTFE. The orientation of polymer chains and concentration of rigid amorphous phase are bigger than in bulk PTFE but smaller than in polymer described in ref. [66]. The films deposited by EVD+ RF LTP were more stable during annealing due to the presence of crosslinks. However film 28 was not less stable than film 17, which has many more crosslinks. Perhaps film 28 has polymer chains with a bigger molecular mass. Perhaps even a small quantity of crosslinks in film 28 significantly increased its stability. However, a comparatively small quantity of crosslinks did not prevent material advance toward an equilibrium state at annealing. Polymer chains became more oriented in perpendicular direction, thus increasing film hardness. Film 29 structure became more ordered.

The structure of PTFE films has several levels of organization: starting from the formation of polymer chains by secondary polymerization on the substrate surface (molecular mass, branching, crosslinking, free bonds, defects, chains orientation), then the formation of structure on a nanolevel (ensemble of crystalline and amorphous domains) and a supermolecular structure (visible by AFM on the surface of film 17). PTFE chains can arrange in fibrils with diameter of about 6 nm. These fibrils are collected in a rod-like structure.<sup>[67]</sup> However, this structure was formed by a crystal phase. The rotating and fixed films were grown under conditions with different ratio between thermodynamics and kinetics. The deposition rate was bigger three times for the fixed films, the supply of the new fluorofragments was constant, thus

limiting the time for fragment to find a partner for reaction and shifting the film structure from the equilibrium one. The rotated film had partial time for equilibrium growth while the film was out of the deposition zone during the EVD process. During EVD + LTP, a few smaller active fragments can participate in film growth even in a shielded zone dependent on RF power and pressure. The postpolymerization of monomer after LTP plays an important role in film structure formation.<sup>[68]</sup> The higher the pressure of perfluorinated fragments and the higher the RF power, the greater part of the film grown in shielded zone during EVD+LTP. Therefore, rotation of the substrate led to a more equilibrium film structure during EVD, while during EVD + LTP the rotation led to a more shift of the structure from equilibrium. The conclusions made concerning growth mechanisms and film structure evolution from a comparison of IRS only of the films deposited in ref. [52] are not correct: the AFM images of those films and the images presented in this paper are quite different, indicating a different organization of film material, suggestive of a different growth mechanism. During formation of bulk PTFE, long molecules are already present, which are free to form crystals with folded chains and separate amorphous phase. During film growth under the influence of a substrate surface with certain physical–chemical properties (in particular, surface energy bigger than PTFE), the chains are formed from the addition of small molecules to an already grown first PTFE layer. Therefore, the chains can grow in the direction of fragment supply—perpendicular to the substrate surface.<sup>[16]</sup> By such mechanism, the PTFE films with polymer chains oriented mainly in the direction perpendicular to the surface of substrate even in amorphous phase were grown. The tie molecules are many that is why the interphase boundaries between the crystal and amorphous phases with only weak interactions are small. These peculiarities in the film structure made PTFE films significantly harder than bulk PTFE.

The roughness of the film surface and refractive index are mainly dependent on the pressure of the gas phase. The RF LTP decreased roughness at a low pressure and increased at a high pressure. The refractive index of the films varied in the 1.15–1.38 range. The absorption coefficient also varied, in two cases becoming almost zero. The molecular structure and chemical composition of transparent PTFE films were close to the structure of bulk PTFE. A higher concentration of amorphous phase in the films reduced light scattering on microcrystals. As films 16 and 17 revealed almost no absorption (no scattering either), the crystals in the films were smaller than 10 nm in size (if any). The absorption coefficient at 632 nm for the deposited films was about ten times smaller than for bulk PTFE<sup>[69]</sup> in the z-direction, thus confirming no light scattering centers in the films. The absorption coefficient in direction parallel to the surface was even smaller. Orientation of the polymer molecules and anisotropy of the refractive index were controlled by deposition conditions. A higher  $n$  and  $k$  perpendicular to the substrate surface direction for all films shows a preferential perpendicular orientation of polymer chains. In the models used, the fitting of the experimental spectral dependencies  $\psi$  and  $\Delta$  for films 17 and 18 occurs with a larger error compared to other films and leads to incorrect results. This indicates a more complex structure of films 17 and 18, confirmed by IRS. More complex optical model is required. Perhaps films 17 and 18 contain nanodomains of four phases. These

phases have no clear interphase boundaries as in bulk PTFE due to tie molecules and crosslinks.

The optimal properties of the PTFE film are dependent on their application: on smooth surface for optics and rough surface for liquid repelling use. For optical sensors, the films with necessary porosity and refractive index can be obtained. To produce high-quality films with the required properties for specific applications, the sum of all the deposition conditions should be explored to derive the optimal sum of these conditions.

### 3. Conclusions

Varying the deposition conditions, pressure of perfluorinated gas and RF LTP power, the PTFE films with different refractive indices, extinction coefficients, structure, morphology, and hardness were produced. The sum of deposition conditions influenced film structure and properties in a complex manner, but the structure and chemical composition of most of the films were close to the bulk PTFE and different from the structure of perfluoro“polymer” films produced by classical LTP. Films produced with EVD and EVD + low power RF plasma were completely transparent over UV-vis–NIR regions. Their refractive indices were varied in the range from 1.15 to 1.38 dependent on deposition parameters. The optical properties of the produced films were close to properties of industrial Teflon-FEP films and better than that of PTFE films. The optical parameters of the PTFE films produced with EVD + low power RF plasma were more stable than produced by EVD. The hardness of the films was several times bigger than the hardness of the bulk PTFE. These valuable properties of films can be explained by the formation of many tie molecules oriented preferably perpendicular to the substrate surface, thus making the film material mainly amorphous with fixed interphase boundaries.

### 4. Experimental Section

**Fabrication of Thin PTFE Films:** The pieces of bulk PTFE made in the USSR were used. A vacuum installation UVN-74 with an evaporator for polymer heating and treatment of gases with a cloud of accelerated electrons, as described in refs. [11, 16] was used for depositions. Advanced Energy Caesar 403 (40.68 MHz) with integrated power control (0–300 W) was used for LTP generation. Starting pressure in the chamber was  $10^{-5}$  mbar. The pressure of emitted gaseous fragments was controlled by temperature of the stainless crucible filled with PTFE and was measured with Pfeiffer vacuum GmbH. The deposition rate was controlled by means of a quartz microbalance Sigma. Films were deposited on polished slides of fused silica and silicon (Si) at an ambient temperature. Some films were deposited inside a glass tube with classical plasma ignited by 1 kV 50 Hz at a pressure of PTFE decomposition products  $1 \times 10^{-1}$  to  $1 \times 10^{-2}$  mbar.<sup>[29]</sup> PTFE films with thickness from 50 to 1000 nm were produced. All the films were made in two sets, each pair of samples in one run: one set was studied in ISP, Kyiv, the second twin set was studied in Szczecin and Wildau Technical Universities. Scheme of deposition installation and processes is shown in **Figure 9**. The small difference in film thickness in set pairs was expected. Annealing was made in Thermo Scientific Cimarec oven at 80 °C for 1 h in a nitrogen atmosphere.

**Optical Measurements and Calculations:** Optical spectra of the films were recorded using one beam spectrometer StellarNet. Lambda 1050 UV/VIS/NIR spectrophotometer (Perkin-Elmer) was used for spectra recording in the extended range. Refractive index at 632.8 nm wavelength was measured by laser ellipsometer LEF-3 M (Ukraine). The thickness and

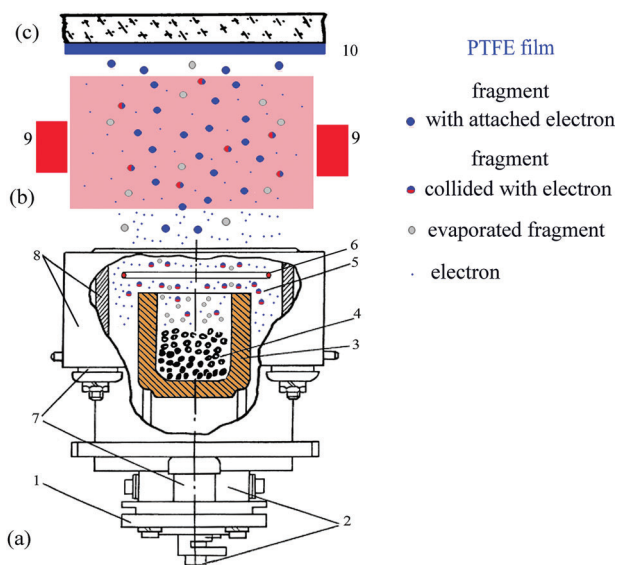


**Figure 9.** Scheme of deposition of PTFE films. a) Industrial evaporator-activator: 1) holder of evaporator, 2) support of the crucible, 3) heated crucible, 4) PTFE granules, 6) ring tungsten cathode, 7) ceramic isolators, 8) shields. b) 9) RF electrodes and LTP between them. c) 10) Substrate with growing PTFE film.

refractive index  $n(\lambda)$  of PTFE films were estimated using spectroscopic ellipsometer SE-2000 (Semilab). For each sample, ellipsometric angles ( $\Psi$ ,  $\Delta$ ) were measured in the 250–2100 nm wavelength range and angles of incidence of 65°, 70°, 75°. Modeling was used to derive optical constants using the experimental  $\Psi$  and  $\Delta$  data. For dielectric films, Forouhi–Bloomer (FB) had suggested a quantum mechanical dispersion model. This model was in the frame of Kramers–Kronig dispersion relations. By using the FB approximation models for the refractive and extinction indices  $n$  and  $k$ , the spectral fitting of ellipsometric angles ( $\Psi$ ,  $\Delta$ ) were performed to minimize the mean-square error between the measured and calculated ellipsometric data. When choosing a model, the AFM data about surface roughness were used. A multilayer model of the interface layer and bulk PTFE on Si substrate was chosen. The interface layer (root mean squared roughness) was analyzed by using the Bruggeman effective medium approximation model. The FB dispersion model described the bulk material of PTFE film. The model used considered the PTFE film as isotropic. Refractive and extinction indices were measured by spectroscopic ellipsometer SENresearch SE 800 DUV (Sentech Instruments, Berlin-Adlershof, Germany). The anisotropic refractive index  $n$  and extinction coefficient  $k$  were measured in the wavelength range from 300 to 980 nm at angles of incidence of 50°, 60°, 70°. A uniaxial anisotropic layer model was used, in which the optical axis was perpendicular to the sample surface. The PTFE films were modeled as Cauchy layers.

Film structure was analyzed by attenuated total reflection Fourier infrared spectroscopy (Lumos, Bruker, USA). 256 scans at a resolution of 4  $\text{cm}^{-1}$  were carried out for each sample in two different places. All spectra were taken in the 4000–400  $\text{cm}^{-1}$  wavenumber range, but the results were presented in a region of interest, i.e., 1800–400  $\text{cm}^{-1}$ . For all spectra, the baseline correction procedure was performed in Origin software. To determine the change of individual bands' intensity, the deconvolution of the 1800–800  $\text{cm}^{-1}$  region was performed using MagicPlot software. The fitting with Gaussian peaks was applied.

**Measurements of Film Properties:** The XPS were obtained using Mg K $\alpha$  ( $h\nu = 1253.7$  eV) radiation with a Prevac (Rogów, Poland) system equipped with a Scienta SES 2002 electron energy analyzer operating at constant transmission energy ( $E_p = 50$  eV). The samples were glued to a molybdenum holder. During measurements, a pressure in the chamber was  $1 \times 10^{-9}$  mbar.

The morphology of the films was studied with an AFM Nanoscope IIIa Dimension 3000 at room temperature in a tapping mode using Si tips of the 8 nm tip apex radius. The correct film thickness was measured by AFM tip. Data were processed using WSxM 5.0 and Gwyddion software. 3D images were presented with a real space scale of axis (the same scale for  $X Y Z$ ). Mechanical properties of the films were measured using a Si tip with its apex radius of 30 nm. Cantilever spring constant was 42  $\text{N m}^{-1}$ . The shape of the tip apex was controlled before and after measurements. Hardness of the film was determined as a ratio of maximum loading force to contact area at a given penetration depth. The Young's modulus was determined using the fitting of the initial part of a loading curve by the Hertz model of elastic contact.

Dynamic contact angle measurements (sessile drop shape analysis) of the PTFE surfaces were performed using a Krüss DSA 100 Drop Shape Analyzer goniometer equipped with a camera and recording system. The measurements were conducted by placing a 2  $\mu\text{L}$  drop of ultrapure water on the surface, followed by increasing the volume to 7  $\mu\text{L}$  (advancing contact angle,  $\theta_a$ ) and then decreasing back to 2  $\mu\text{L}$ , at a flow rate 0.33  $\mu\text{L s}^{-1}$ . The average dynamic contact angle was calculated from two measurements. Reference material was polished prior to measurement.

## Supporting Information

Supporting Information is available from the Wiley Online Library or from the author.

## Acknowledgements

Thanks go to Dr. V. Ksianzou (D) for the optical transmission spectra in wide spectral range and A. Gritsenko (UK) for English editing, to Philipp Schwarz Initiative of the Alexander von Humboldt Foundation for funding the stay of K.G. at TH Wildau.

Open access funding enabled and organized by Projekt DEAL.

## Conflict of Interest

The authors declare no conflict of interest.

## Data Availability Statement

The data that support the findings of this study are available in the Supporting Information of this article.

## Keywords

deposition in vacuum, multiphase structure formation, optical properties, plasma, polytetrafluoroethylene thin films

Received: October 27, 2022  
Revised: January 2, 2023  
Published online: February 19, 2023

- [1] Z. Seres, A. Galonsky, K. Leki, J. J. Kruse, P. D. Zecher, *J. Ocul. Pharmacol. Ther.* **1994**, *33*, 3031.
- [2] N. Field, J. E. Bazin Andrew, H. A. McInnes, *Proc. SPIE* **1999**, *3492*, 964.
- [3] C. Li, H. Jiang, *Micromachines* **2014**, *5*, 432.
- [4] P. D. Keathley, J. T. Hastings, *J. Vac. Sci. Technol., B: Nanotechnol. Microelectron.: Mater., Process., Meas., Phenom.* **2008**, *26*, 2473.

- [5] G. V. Dorozhynska, G. V. Dorozhynski, V. P. Maslov, K. P. Grytsenko, Y. V. Kolomsarov, P. M. Lytvyn, T. P. Doroshenko, *Optoelectron. Semi-cond. Tech.* **2019**, *54*, 88.
- [6] T. Mak, R. J. Westerwaal, M. Slamán, H. Schreuders, A. W. van Vugt, M. Victoria, C. Boelsma, B. Dam, *Sens. Actuators, B* **2014**, *190*, 982.
- [7] B. Wang, C. J. Ruud, J. S. Price, H. Kim, N. C. Giebink, *Nano Lett.* **2019**, *19*, 787.
- [8] K. Isakov, C. Kauppinen, S. Franssila, H. Lipsanen, *ACS Appl. Mater. Interfaces* **2020**, *12*, 49957.
- [9] V. Karre, *Master Thesis*, University of Kentucky, Lexington, KY **2009**.
- [10] V. V. Petrov, A. A. Kryuchin, I. V. Gorbov, Y. O. Borodin, J. L. Briks, V. V. Kurdiukov, Y. L. Slominskii, O. I. Tolmachev, K. P. Grytsenko, *Patent of Ukraine No. 110143*, **2015**.
- [11] K. Grytsenko, V. Ksianzou, Y. Kolomsarov, P. Lytvyn, B. Dietzel, S. Schrader, *Surface* **2021**, *4*, 66.
- [12] V. M. Yashchuk, K. P. Gytsenko, S. Schrader, O. Navozenko, *Bull. Kyiv Univ.* **2017**, *2*, 109.
- [13] J. Y. Shin, T. W. Kim, G. Y. Kim, S. M. Lee, J. W. Hong, *Trans. Electr. Electron. Mater.* **2017**, *18*, 89.
- [14] J. Roh, I.-T. Cho, H. Shin, G. Woo Baek, B. Hee Hong, J.-H. Lee, S. H. Jin, C. Lee, *Nanotechnology* **2015**, *26*, 455201.
- [15] P. Zhang, X. Xu, Y. Dang, S. Huang, X. Chen, B. Kang, S. R. P. Silva, *ACS Sustainable Chem. Eng.* **2016**, *4*, 6473.
- [16] K. P. Gritsenko, A. M. Krasovsky, *Chem. Rev.* **2003**, *103*, 3607.
- [17] K. P. Gritsenko, A. Capobianchi, A. Convertino, J. Friedrich, R. D. Schulze, V. Ksensov, S. Schrader, in *Polymer Surface Modification and Polymer Coatings by Dry Process Technologies* (Ed: S. Iwamori), Research Signpost, India **2005**, p. 85.
- [18] H. Takele, A. Kulkarni, S. Jebri, V. S. K. Chakravadhanula, C. Hanisch, T. Strunskus, V. Zaporozhchenko, F. Faupel, *J. Phys. D: Appl. Phys.* **2008**, *41*, 125409.
- [19] S. Tripathi, R. De, K. D. Rao, S. M. Haque, B. K. Goud, C. Prathap, J. S. Misal, M. M. Patidar, V. Ganesan, N. K. Sahoo, *Adv. Polym. Technol.* **2018**, *37*, 2774.
- [20] M. Psarski, D. Pawlak, J. Grobelny, G. Celichowski, *J. Adhes. Sci. Technol.* **2015**, *29*, 2035.
- [21] I. Muzammil, Y. P. Li, X. Y. Li, D. K. Dinh, M. Imran, H. Sattar, M. K. Lei, *J. Coat. Technol. Res.* **2020**, *17*, 621.
- [22] A. Carletto, J. P. S. Badyal, *J. Phys. Commun.* **2017**, *1*, 055024.
- [23] S. Pedram, H. R. Mortahe, H. Fakhouri, X. Arefi-Khonsari, *Plasma Chem. Plasma Process.* **2017**, *37*, 223.
- [24] E. M. Tolstopyatov, *Ph.D. Thesis*, Metal-Polymer Research Institute, Belarus **2017**.
- [25] J. Piwowarczyk, R. Jędrzejewski, D. Moszynski, K. Kwiatkowski, A. Niemczyk, J. Baranowska, *Polymers* **2019**, *11*, 743.
- [26] N. Yi, S. Bao, H. Zhou, Y. Xin, A. Huang, Y. Ma, R. Li, P. Jin, *Front. Mater. Sci.* **2016**, *10*, 320.
- [27] R. Acharya, D. Gündler, T. Breuer, G. Schmitz, H. Klauk, G. Witte, *J. Mater. Chem. C* **2021**, *9*, 270.
- [28] K. P. Gritsenko, *Russ. J. Gen. Chem.* **2009**, *79*, 642.
- [29] K. P. Grytsenko, *Ph.D. Thesis*, Metal-Polymer Research Institute of National Academy of Sciences of Belarus, Gomel, Belarus **1997**.
- [30] R. H. French, J. M. Rodríguez-Parada, M. K. Yang, R. A. Derryberry, M. F. Lemon, M. J. Brown, C. R. Haeger, S. L. Samuels, E. C. Romano, R. E. Richardson, in *Proc. 34th IEEE Photovoltaic Specialists Conf. (PVSC)*, IEEE, Piscataway, NJ **2009**, pp. 000394–000399.
- [31] N. Ohnishi, R. Nomura, T. Nakamura, H. Nishida, *Jpn. J. Appl. Phys.* **2016**, *55*, 02BB04.
- [32] S. Iwamori, K. Noda, *Mater. Lett.* **2012**, *66*, 349.
- [33] A. Zhuang, R. Liao, S. C. Dixon, Y. Lu, S. Sathasivam, I. P. Parkin, C. J. Carmalt, *RSC Adv.* **2017**, *7*, 29275.
- [34] R. A. Alawajji, G. K. Kannarpady, A. S. Biris, *Appl. Surf. Sci.* **2018**, *444*, 208.
- [35] S. Tripathi, S. M. Haque, K. D. Rao, R. De, T. Shripathi, U. Deshpande, V. Ganesan, N. K. Sahoo, *Appl. Surf. Sci.* **2016**, *385*, 289.
- [36] M. Gauch, M. Ließmann, H. Ehlers, D. Ristau, in *Optical Interference Coatings* (Eds: M. Tilsch and D. Ristau), Optica Publishing Group, Washington, DC **2013**, ThA.2.
- [37] E. Cho, S. Song, M. Kim, J.-S. Park, S. Park, S.-J. Lee, *Polym. Adv. Technol.* **2022**, *33*, 3470.
- [38] S.-W. Kim, C. Kang, H.-K. Kim, *Adv. Mater. Interfaces* **2022**, *9*, 2101823.
- [39] K. K. S. Lau, J. A. Caulfield, K. K. Gleason, *J. Vac. Sci. Technol., A* **2000**, *18*, 2404.
- [40] R. De, S. M. Haque, R. Singh, C. B. Basak, S. Jena, J. S. Misal, D. D. Shinde, T. Som, K. D. Rao, *J. Coat. Technol. Res.* **2021**, *18*, 173.
- [41] S. R. Lee, M. R. Kim, E. H. Jo, K. Yoon, *High Perform. Polym.* **2016**, *28*, 131.
- [42] S. H. Wemple, M. Didomenico, *Phys. Rev. B* **1971**, *3*, 1338.
- [43] K. Tanaka, *Thin Solid Films* **1980**, *66*, 271.
- [44] H. Tichá, L. Tichý, *J. Optoelectron. Adv. Mater.* **2002**, *4*, 381.
- [45] C. Y. Liang, S. Krimm, *J. Chem. Phys.* **1956**, *25*, 563.
- [46] R. E. Moynihan, *J. Am. Chem. Soc.* **1959**, *81*, 1045.
- [47] D. Sianesi, G. Caporiccio, *Makromol. Chem.* **1963**, *60*, 213.
- [48] G. Dube, H. Kriegsmann, *Z. Chem.* **1965**, *5*, 421.
- [49] H. W. Starkweather, Jr., R. C. Ferguson, D. B. Chase, J. M. Minor, *Macromolecules* **1985**, *18*, 1684.
- [50] C. Quarti, A. Milani, C. Castiglioni, *J. Phys. Chem. B* **2013**, *117*, 706.
- [51] Y. Zhang, T. Katoh, A. Endo, *J. Electron Spectrosc. Relat. Phenom.* **2001**, *119*, 247.
- [52] A. A. Rogachev, S. Tamulevicius, A. V. Rogachev, M. A. Yarmolenko, I. Prosycevas, *Appl. Surf. Sci.* **2009**, *255*, 6851.
- [53] G. Masetti, F. Cabassi, G. Morelli, G. Zerbi, *Macromolecules* **1973**, *6*, 700.
- [54] N. Nagai, H. Okada, T. Hasegawa, *AIP Adv.* **2019**, *9*, 105203.
- [55] M. Schott, *Synth. Met.* **1994**, *67*, 55.
- [56] P. A. Luchnikov, A. A. Rogachev, A. P. Luchnikov, *Nano Microsyst. Tech.* **2007**, *10*, 6.
- [57] E. K. Kosgoy, *Graduate Thesis*, Missouri State University, MI, USA **2015**.
- [58] K. P. Grytsenko, P. M. Lytvyn, J. Friedrich, R. D. Schulze, S. Schrader, *Mater. Sci. Eng., C* **2007**, *27*, 1227.
- [59] J. Carneiro De Oliveira, A. Airoudj, P. Kunemann, F. Bally-Le Gall, V. Roucoules, *SN Appl. Sci.* **2021**, *3*, 656.
- [60] Y.-L. Yu, X.-Q. Xu, C.-D. Lu, T.-H. Zhang, Y. Ma, *Thin Solid Films* **2020**, *712*, 138302.
- [61] A. F. Michels, P. A. Soave, J. P. Nardi, L. G. Jardim, S. R. Teixeira, D. E. Weibel, F. Horowitz, *J. Mater. Sci.* **2016**, *51*, 1316.
- [62] J. D. Miller, S. Veerasaneni, J. Drelich, M. R. Yalamanchili, *Polym. Eng. Sci.* **1996**, *36*, 1849.
- [63] K. Grytsenko, Y. Kolomsarov, P. Lytvyn, I. Lebedyeva, E. Vashchilina, *Surf. Topogr.: Metrol. Prop.* **2021**, *9*, 5006.
- [64] G. Calleja, A. Jourdan, B. Ameduri, J.-P. Habas, *Eur. Polym. J.* **2013**, *49*, 2214.
- [65] S. Wietzke, C. Jansen, M. Reuter, T. Jung, J. Hehl, D. Kraft, S. Chatterjee, A. Greiner, M. Koch, *Appl. Phys. Lett.* **2010**, *97*, 022901.
- [66] M. Polinska, A. Rozanski, A. Galeski, J. Bojda, *Macromolecules* **2021**, *54*, 9113.
- [67] G. J. Puts, P. Crouse, B. M. Ameduri, *Chem. Rev.* **2019**, *119*, 1763.
- [68] J. Friedrich, *Plasma Process. Polym.* **2011**, *8*, 783.
- [69] S. S. Gusev, I. S. Malashchenko, M. M. Kabaev, L. E. Starovoitov, *High Mol. Compd.* **1992**, *A34*, 78.